Synthetic view of two-dimensional aggregation

Abdelwahab Ghazali
Groupe de Physique des Solides, UMR 7588-CNRS, Universités Paris 6 et Paris 7, Campus Boucicaut, Paris 15, France

Jean-Claude Serge Lévy
Laboratoire de Physique Théorique de la Matière Condensée EA 2382, Pôle MPQ FDR 2437, Université Paris 7, case 7020, 75251 Paris 05, France

(Received 2 July 2003; revised manuscript received 8 March 2004; published 17 June 2004)

Extensive Monte Carlo simulations using short-range and medium-range interactions reveal the existence of quasisteady out-of-equilibrium phases in two-dimensional (2D) atom or cluster aggregation at different coverages namely fractal-type, dendrites, compact islands with faceted or rough boundaries, as well as gas or fluid phases. Different aggregation processes are identified. For medium-range effective pair potentials such as the one used for copper atoms, 2D liquid droplets are found.

DOI: 10.1103/PhysRevE.69.061405 PACS number(s): 61.43.Hv, 68.43.Hn, 05.65.+b, 05.70.Ln

I. INTRODUCTION

The recent progress in depositing a large number of particles with well defined selected sizes over a surface using convenient low fluxes [1] as well as the progress in scanning tunneling microscopy at the atomic scale [2] enabled experimentalists to observe several morphologies in two-dimensional (2D) aggregation such as fractals and random dendrites [3,4]. At higher 2D coverage the observation of islands with various shapes is well known [3,5]. From the theoretical point of view, models of diffusion limited aggregation (DLA) [6], and diffusion limited cluster aggregation [7] enabled physicists to understand the existence of fractal shapes in the framework of a simple model of sticking which precludes further relaxation or separation from the cluster. Recently some approaches of internal cluster relaxation were introduced [8] in order to take into account the observed existence of different fractal shapes.

Here, in a more general approach of 2D aggregation we propose to use a classical Monte Carlo (MC) method with simple effective pair potentials to describe the thermal relaxation which can either free freshly deposited particles or aggregate them as well. Thus a synthetic view is expected from this approach. As recently shown [9], the MC approach is well suited to simulate out-of-equilibrium quasisteady states because of its simplified dynamics. The great advantage of the MC method in a canonical ensemble stems from the introduction of a thermal bath at a given temperature T. It enables us to simulate controlled thermal fluctuations without dealing with the energy conservation rule during the motion as required in the standard molecular dynamics approach.

For the sake of clarity an initial random particle configuration within a flat disk deposited on a smooth substrate at a given coverage $\theta<1$, i.e., under one monolayer is introduced in the simulation before starting the relaxation process. Here the particle motion is entirely due to the relaxation process as in pulsed laser deposition [10] and not due to competition between the incoming flux and relaxation processes as it occurs in a continuous particle deposition flux, or in a spinodal transition [11]. The atomic structure of the substrate is neglected for the sake of simplicity and generality. This is well justified in the experimental cases of deposition over a liquid surface or over an amorphous surface, such as amorphous carbon and silica surfaces [12]. Of course introducing a specific substrate structure would lead to deposit structures which are either commensurate or incommensurate with the substrate as it has often been observed in the case of high coverage [3]. The presence of a substrate would also produce preferred crystallographic directions of the deposit which lead to long range orientation correlations [13] and to long range elastic interactions of the deposit through the substrate [14] which in turn may lead to complex labyrinthine deposit structures [15]. All these specific texture points are neglected in the present general approach.

Thus the goal of the present paper is to study the patterned structures at different temperatures obtained from MC simulations with simple short-ranged pair potentials in order to understand the various obtained configurations at equilibrium or out of equilibrium. The initial concentration plays a role in defining several relaxation processes since for large concentrations, particles interact together from the very beginning and clusters are close to each other while for low concentrations there is almost no interaction and the interaction between particles appears only after a long diffusion time. Obviously diffusion increases very much with temperature and the relaxation processes for aggregated particles are also very sensitive to temperature. Thus temperature plays a key role. Finally it is interesting to consider interactions with different ranges and to examine their influence on the obtained patterned structures and on the adsorbate energetics such as the classical monotonous dependence of surface tension on interaction range. This remark suggests that results are general for very short ranged potentials and that some specificities must appear for potentials with a larger interaction area.

In the following, Sec. II deals with the model used for the chosen potentials and MC method. The analysis of the different patterns is reported in Sec. III and remarks and conclusions are given in Sec. IV.

 ©2004 The American Physical Society

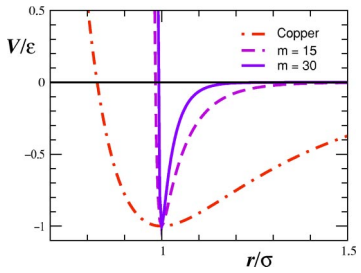

FIG. 1. The three potential wells in normalized units: $m=30$, $m=15$, and copper.

II. MODEL

A. The pair potentials

Here we use as simple effective pair potentials a set of generalized Lennard-Jones pair potentials $V_{n,m}(q)=(q^n-nq)/(n-1)$ with $q=(\sigma/r)^m$ where σ is the optimal pair interparticle distance and r the interparticle distance. The potential well depth is taken as unit energy. The exponents m and nm characterize the interparticle attractive and hard core repulsive terms, respectively. For atoms these exponents are adjusted to the solid state elastic and energetic properties [16]. For instance $m=5$ and $n=1.1$ are deduced for copper [17]. For large particles, i.e., clusters, made of several atoms which are assumed here to be identical disks of diameter σ, the energy well at the cluster surface is just due to edge atoms and ultimately to a single atom while the minimum interparticle distance is equal to $D\sigma$ with $D>1$. To account for this effect, we use the following approximate scaling rules. The effective attractive exponent m' for the cluster is $m'=Dm$, m being the atomic attractive exponent. Thus the use of a large value of the exponent m for cluster-cluster interaction amounts to reduce the interaction range to a very local one as compared to the cluster diameter. The same argument holds for the repulsive exponent n related to hard core cluster-cluster repulsion. Practically we consider here the cases with $m=15$, $n=10$ and $m=30$, $n=10$ in order to deal with disk-shaped clusters of a few to tens atoms, respectively. Thus the choice of generalized Lennard-Jones pair potentials is justified since these potentials can describe very short ranged potentials as well as medium-range potentials such as copper and lead potentials where they give realistic surface structures for Pb/Cu (100) [17]. We also treat the aggregation of copper atoms as the aggregation of soft-potential metallic atoms. Another application could be the colloid-colloid interaction which has been well studied experimentally and theoretically [18].

Fig. 1 shows in reduced units the considered pair potentials, two short-range potentials ($m=15$, $n=10$; $m=30$, $n=10$) and the medium-range potential of copper.

B. MC simulations

The key feature of our simulations comes from the temperature dependence of the energy per particle [Fig. 2(a)]. These curves are obtained after several millions of Monte Carlo steps (MCS) at each temperature, starting from random particle configurations of 10 000 particles with a given coverage θ. We have studied samples with various coverages: $\theta=0.05$, 0.10, 0.16, 0.23, 0.30, 0.39, 0.50, 0.60, and 0.80. In the low temperature regime ($T<0.2$), all curves show an energy decrease upon heating which is a signature of an out-of-equilibrium relaxation process, since in equilibrium systems, the energy increases with temperature leading to a positive specific heat. This out-of-equilibrium feature is illustrated by the low temperature curves ($T=0.01$ and $T=0.1$) in Fig. 2(b) where the energy is slightly decreasing during relaxation, even after 10^7 MCS. Notice, however, that after such long relaxations, the system is in a quasiequilibrium state, i.e., its properties remain essentially unchanged after further relaxation. In particular, the fractal or dendritic nature of the sample persists for those temperatures, respectively (see below). This very long-time relaxation has been studied on smaller samples with 500 and 1000 particles. After 10^9 MCS no true equilibrium state is obtained. In the case of very short ranged potentials the convergence speed does not practically depend on the number of particles of the sample for a given coverage θ. This has been checked from numerical comparisons. This is due to the very short-range nature of these potentials which are practically free from finite size effects. On the other hand, the energy per particle is a decreasing function of particle concentration due to more branching and more connectivity as shown below.

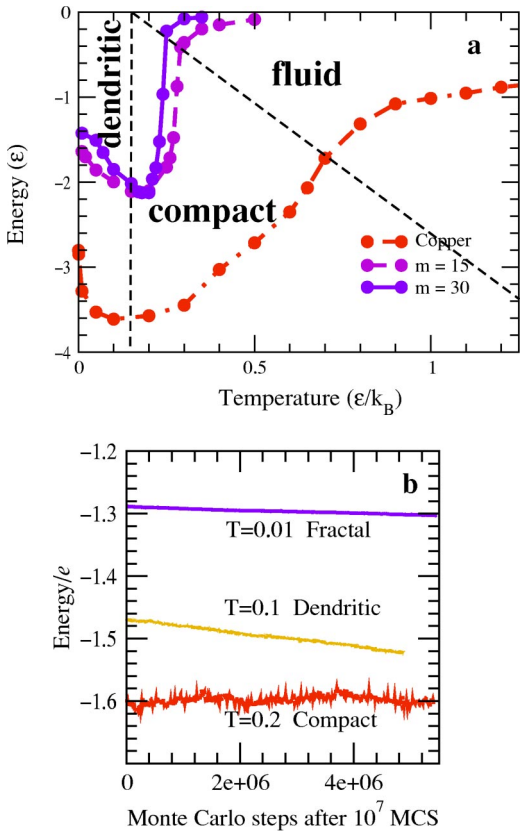

FIG. 2. The energy per site during relaxation: (a) vs temperature after 10^6-10^7 MCS, for the three potentials with coverage $\theta=0.23$; (b) vs the number of MC steps after a run of 10^7 MCS, at temperatures $T=0.01$, $T=0.1$, and $T=0.2$, for $m=30$-potential with $\theta=0.05$.

The energy-temperature curves shown in Fig. 2(a) have a common shape with an out-of-equilibrium regime, as de-

scribed above, followed by a minimum and further a rapid and large increase of energy which is usually associated with a first order phase transition. In the high temperature quasi-steady-state regime, the systems are in a fluid state. For short-range interactions ($m=30$ and $m=15$), the energy per particle at high temperature is practically zero which is the signature of an almost noninteracting gas, while it is about -0.56 for the medium-range copper interaction after 4×10^7 MCS, which is an evidence of a 2D liquid as it results from structure analysis (see below). The shape similarity of energy-temperature curves [Fig. 2(a)] is the first evidence of a universal behavior for two-dimensional aggregation irrespective of the interaction range.

III. PATTERNS

A. Fractals

At much low temperature fractal configurations, i.e., ramified structures with a single particle thickness, are obtained for the three considered potentials as shown in Figs. 3(a)–3(c). The size and the degree of ramification of these aggregates strongly depend on the particle concentration as reported in Figs. 3(a) and 3(b). For low concentrations most of the clusters are linear, while for higher concentrations more and more branches and closed loops appear and small compact parts with a triangular arrangement of particles.

The aggregation process is easily retrieved by comparing successive snapshots. It results not only from individual particle aggregation but also from cluster-cluster aggregation when migrating clusters aggregate. This is rather different from the standard DLA process. Small clusters are more mobile than large clusters; they undergo translations, rotations, deformations, and vibrations.

For concentrations larger than 30%, triangular lattice parts appear from the very beginning of the relaxation process and are almost not affected by relaxation. There is a percolation threshold, i.e., a concentration for which very large clusters are expanding through the sample. This is seen in Fig. 3(b) for a sample with 39% concentration. For higher concentrations, one main cluster appears with smaller ones. Such ramified structures were observed for Ag deposition on a Pt (111) surface at 75 K at moderate coverage, see, e.g., Fig. 3(d) in Ref. [4].

As the temperature is increased, random dendritic patterns [3], i.e., thick ramified structures appear. The transition temperature between fractal (f) configurations and random dendrites (d) depends on the potential range: $T_{f-d}\approx0.02$ for $m=30$, $T_{f-d}\approx0.01$ for $m=15$, and $T_{f-d}<0.0001$ for copper.

B. Random dendrites

Random dendrites shown in Figs. 4(a)–4(c) have an overall fractal aspect but the width of their branches is larger than one particle diameter and smaller than the cluster size. The thickness of these dendrites are a few interatomic distances as seen in Fig. 4(c). These dendrites have a large domain of existence as seen in Fig. 2(a). Such random dendrites are observed experimentally; see Ref. [3].

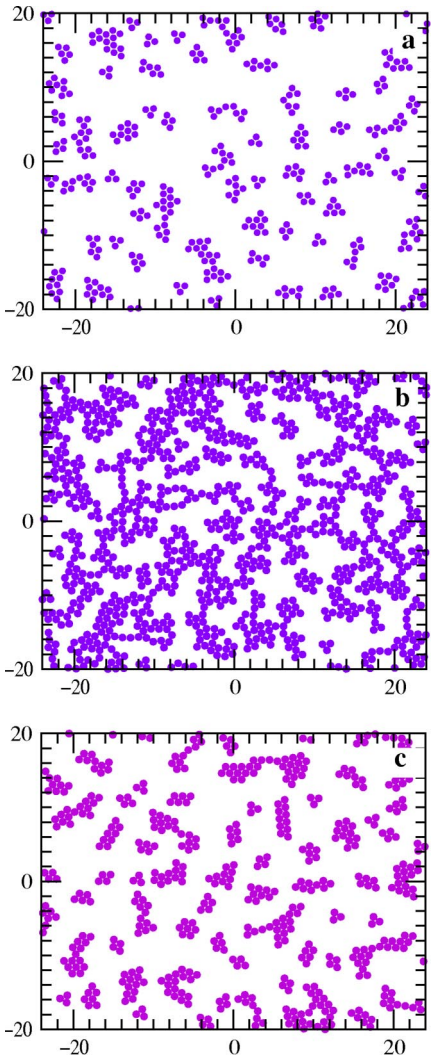

FIG. 3. Fractal-type configurations at $T=0.01$ for short-range potentials: (a) $m=30$ with $\theta=0.16$ after 10 megaMCS; (b) $m=30$ with $\theta=0.39$ after 7.8 megaMCS. Note the practical percolation; (c) $m=15$ with $\theta=0.23$ after 6 megaMCS.

As in fractal regime, the dendrites appear when the energy per particle is a decreasing function of temperature, i.e., in a typical out-of-equilibrium state. The evolution of random dendrites is slow and results from cluster internal deformations, motion, splitting and aggregation, especially when dendrites are small; see Figs. 4(a)–4(c). These dynamic features are consistent with the quasi inexistence of particle thermal detachment in this temperature range. As a result of the aggregation of small units, the number of dendrites decreases during relaxation while the dendrite average size increases. During this growth, depletion regions around large dendrites appear and widen. The motion of large dendrites is quite limited while small dendrites merge together in a coalescence process, and finally with larger dendrites, i.e., in an Ostwald ripening process.

As the temperature is increased further, compact islands appear. The transition temperature between dendrite (d) and compact island (c) phases is only weakly potential dependent: $T_{d-c}\approx0.15$ for all cases including copper. This means

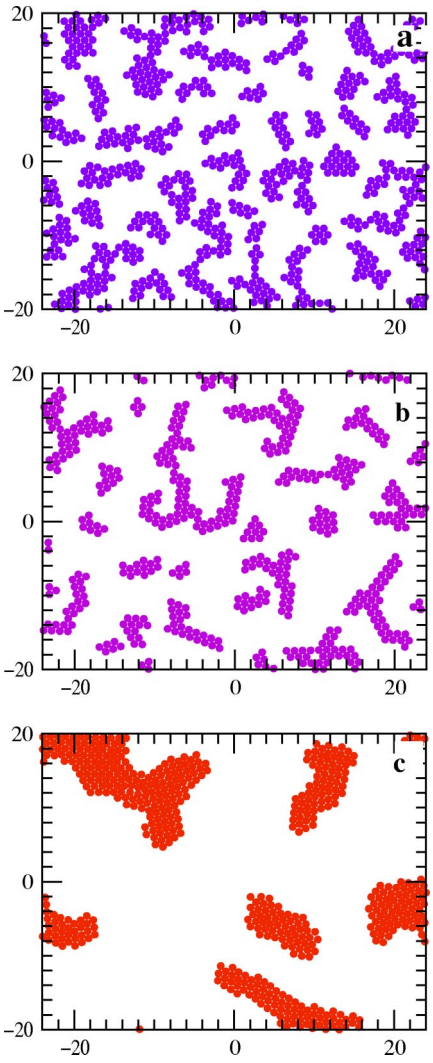

FIG. 4. Random dendrites for: (a) $m=30$-potential at $T=0.1$ with $\theta=0.30$ after 1.5 megaMCS; (b) $m=15$-potential at $T=0.05$ with $\theta=0.23$ after 6.5 megaMCS; (c) copper at $T=0.05$ with $\theta=0.23$ after 1.7 megaMCS.

that the compact island formation is driven by the thermal softening of bonds, especially those located at the cluster edge which are weaker than the inner ones because of the number of interacting neighbors and the available free space.

C. Compact islands

Compact islands with a triangular crystalline structure appear [Figs. 5(a)–5(d)] for $T \geqslant T_{d-c} \approx 0.15$. Their average energy per particle is a weakly increasing function of temperature. This means that this solid phase is close to equilibrium as illustrated in Fig. 2(b) for $T=0.2$ where the long-time average energy per particle is just fluctuating around its mean value without drift. The island morphology and dynamics depend on the interaction range. There is a continuous coexistence of rather large islands, clusters, and single particles, see Fig. 5(a), for local potentials such as in the case of $m=30$, while for soft potentials such as in the case of copper, there is a large temperature range, $0.2 < T < 0.4$, with islands only [Figs. 5(b) and 5(c)]. Such a difference may be understood as follows: at moderate temperature when the thermal energy becomes a sizeable fraction of the potential well depth, a particle can easily escape from the well if narrow, while for wider potentials, the particles cannot escape in a few steps, and free particles are easily captured by a wide potential well.

In the solid phase several island shapes appear. They result from the motion of particles at the island edge. The basic features are displayed in Figs. 5(a)–5(d) with evidence for polygonal and rough boundaries.

1. Hexagonal and triangular islands

At low temperature, island edges are straight lines with a large proportion of hexagonal shapes as seen in Figs. 5(a) and 5(d), in agreement with the experimental observations of hexagonal and triangular islands [3].

For local potentials such as the case of $m=30$ or $m=15$, the transition from compact islands with hexagonal or triangular shapes to a gas phase is very sharp. For soft potentials such as that of copper, there is a transition from faceted smooth (s) islands to rough (r) islands which starts at $T_{s-r} \simeq 0.28$.

2. Rough islands

At higher temperatures, the island edges become rougher and rougher as seen in Figs. 5(b) and 5(c), leading finally to sublimation due to particle escape at the edge. This behavior depends on island size: large islands exhibit smoother and more coordinated edges than small islands, so they undergo sublimation less easily than the latter. Thus sublimation of small islands and condensation on large islands simultaneously occur. This is the Ostwald ripening [19]. There is an intermediate step in which a few large rough islands are surrounded by particles and clusters as seen in Figs. 5(b) and 5(c). In the long run, rough islands finally disappear in an expanding cloud of particles and clusters.

The particle motion strongly depends on the potential range. For medium-range potentials the edge tension involves several inner layers, while for short-range potentials this tension involves the edge particles only. This is the reason why the transition from faceted islands to rough islands is so narrow for local potentials and so extended for a copper medium-range potential. Similarly a stronger edge tension stabilizes a nearly circular shape at the expense of more rectilinear edges [Figs. 5(b) and 5(c)]. This is the reason why in the case of a copper medium-range potential islands are stable over a wide temperature range.

3. Island dynamics versus concentration

The island dynamics is very rich and is well known since Ostwald [19]. At the early stages of island growth for appropriate concentration and temperature, single particles aggregate and soon dimers, trimers, etc. also aggregate. Then numerous islands of different sizes appear. Large islands grow by simultaneously (i) merging together in a coalescence process and by (ii) receiving small clusters and single particles in a sublimation-accretion process, i.e., the Ostwald-type rip-

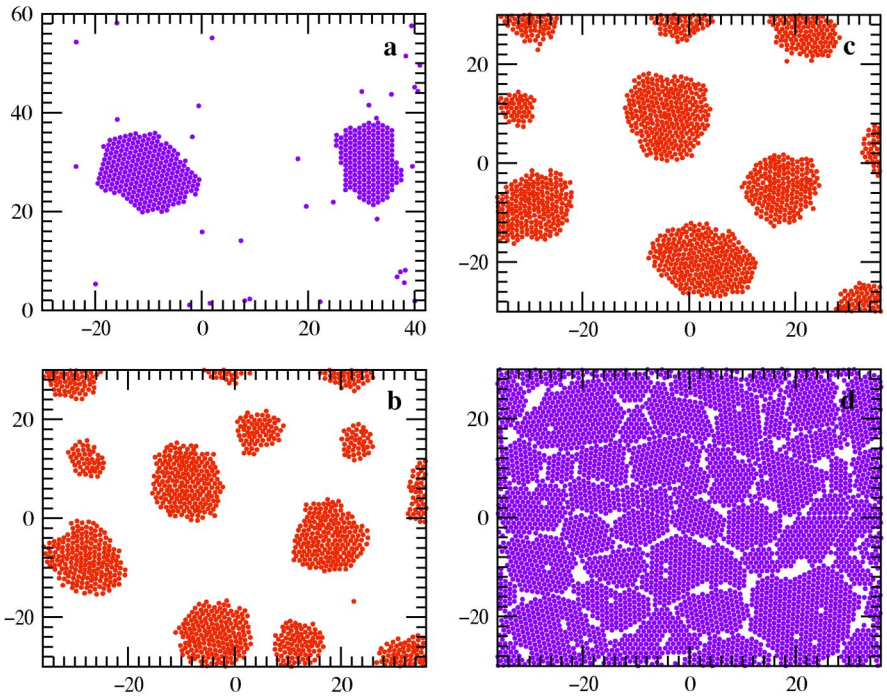

FIG. 5. Compact islands for: (a) $m=30$-potential at $T=0.2$ with $\theta=0.05$ after 16.6 megaMCS; (b) copper at $T=0.3$ with $\theta=0.23$ after 1.4 megaMCS; (c) copper at $T=0.3$ with $\theta=0.23$ after 2.4 megaMCS. Note the island size growth when comparing to (b); (d) $m=30$-potential at $T=0.2$ with $\theta=0.8$ after 5 megaMCS. Note the grain independent crystalline orientation and the presence of vacancies inside the grains.

ening [19]. Both processes are very slow processes since they involve both slow motions of large islands and slow edge reorganization of old and newly aggregated islands. Curiously enough, this size increase occurs even at high temperature, close to the solid-fluid transition where larger and larger islands appear. However, after a long enough MC run these islands disappear due to sublimation for very short-range potentials.

At low concentration, island coalescence does not occur since it involves island motion over large distances which is much slower than single particle motion. Thus Ostwald ripening at low concentration just results from sublimation of small islands and particle condensation into large islands for energetic reasons. At high concentrations, islands are close to each other. So they coalesce easily. This is shown for moderate concentration in Figs. 5(b) and 5(c) where the same sample is shown at two different MC steps. Several small islands coalesce in Fig. 5(c) and one isolated small island remains. At higher concentration, islands coalesce from the very beginning to form larger crystalline polygonal islands which become self organized in a semiordered network [Fig. 5(d)]. The sublimation process is still present with evidence for internal vacancies. The relaxation process is dominated by coalescence.

The next thermal transition is an abrupt first order transition from solid (s) towards gas (g) phase, i.e., a sublimation for local potentials at $T_{s-g}\approx 0.25$ for $m=30$ and $T_{s-g}\approx 0.285$ for $m=15$ and a less abrupt transition towards the liquid phase, i.e., a melting (m), for medium-range potentials, here the copper case with $T_m\approx 0.65-0.7$ as seen in Fig. 2(a).

D. Fluid phases

At higher temperatures fluid phases appear. They are made of mobile individual particles and of mobile clusters of various sizes. All these structures at a given MC step form an expanded cloud as seen in Figs. 6(a)–6(c). When the potential range is increased, clusters of larger size appear. This explains the difference between Fig. 6(a) where the potential is very hard with $m=30$ and Fig. 6(b) where the potential is less hard with $m=15$. In both cases, the fluid phase is a gas.

For the short-range potentials, which lead after very long MC runs to the snapshots reported in Fig. 6(a) and 6(b), the local particle density decreases from the center of the initial disk towards the outside according to a Gaussian distribution, as it occurs in a free 2D random walk from a source located at the origin.

For the medium-range copper potential, the transition from compact islands to fluid phases extends over a large plateau $0.6<T<1.3$ with a potential energy close to -1; see Fig. 2(a). This plateau corresponds to the dense fluid at $T=1.3$ as seen in Fig. 6(c) for 4×10^4 MCS. The sample size expands mainly as a result of 2D spatial expansion at the phase transition, and most of the sample remains confined within a disk. The existence of this dense liquid phase is analyzed with the help of the distribution function of site neighbors reported in Fig. 7. The probability of a site with a given number of neighbors within a distance of three atomic radii is reported in Fig. 7. In our model in 2D, the maximum number of interacting neighbors is 36 in the case of a triangular lattice. In the islands obtained here, this number varies between 18 at the surface and 36 in the island core. This is seen in Fig. 7 for $T<0.65$. From the shape of the distribution function at these temperatures, the island size increases with temperature as reported above. In the temperature range, $0.8<T<1.3$, the average number of neighbors is eight with a Poissonian distribution. At the melting point $T=0.65$ the distribution function of the number of neighbors becomes quite wide. Both liquid and solid states coexist as in a first order transition. Note that with a medium-range potential, close to the melting transition, a few sites with a quasisquare

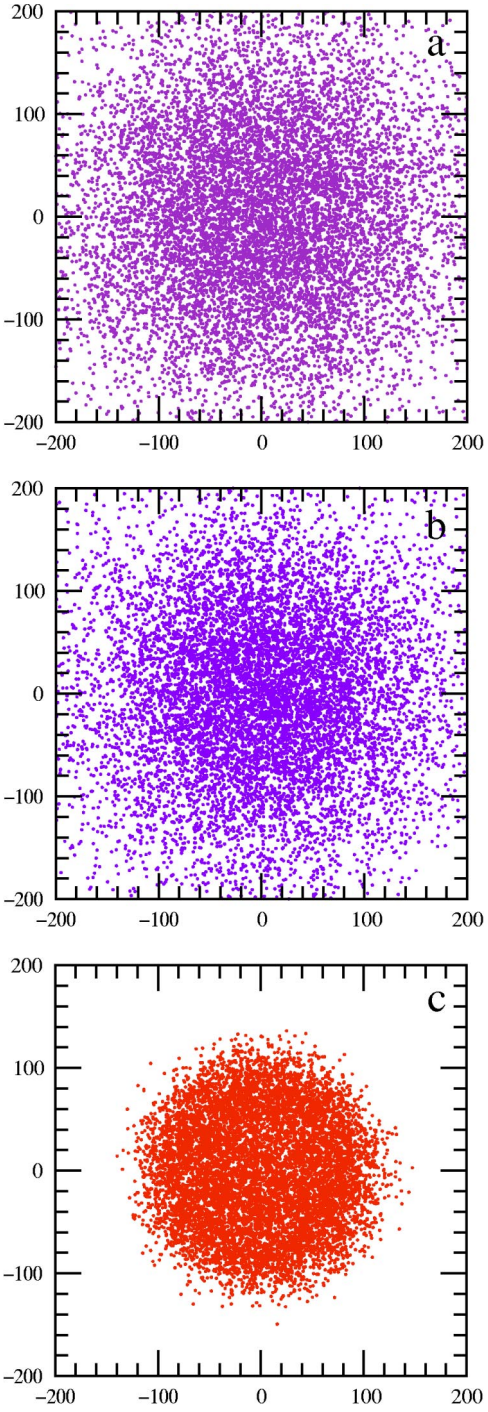

FIG. 6. Fluid phases: (a) gas for $m=30$ at $T=0.35$ after 10 megaMCS. Note the weak energy per site, $E=-0.059$; (b) gas for $m=15$ at $T=0.35$ after 10 megaMCS, $E=-0.197$; (c) liquid copper at $T=1.3$ after 4.4×10^4 MCS. In all cases the initial coverage is $\theta=0.23$.

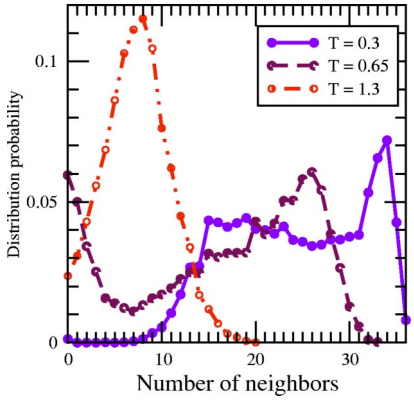

FIG. 7. Copper solid-liquid transition: Normalized distribution probability of the number of site interacting neighbors within a disk of radius three atomic radii at temperatures $T=0.3$ (solid islands), $T=0.65$ (melting point with coexistence of solid islands and liquid) and $T=1.3$ (liquid phase).

symmetry environment appear in the sample. Such configurations seem to be related to their 3D analog, namely the high temperature bcc phase in metals [20].

IV. CONCLUDING REMARKS

In conclusion, by using a simple interaction model for 2D aggregation, we have accounted for a rich variety of patterns and phases as observed experimentally. A schematic "phase diagram" is summarized in Fig. 2(a). The fractal region is too narrow to be shown in this figure but exists. Our model in which diffusion and internal relaxation play major roles could be very suggestive for numerous out-of-equilibrium statistical phenomena such as urban growth [21] where linear villages as well as urban coalescence have been observed long ago. In the case of patterned grounds [22] polygonal networks also appear as in our MC patterns obtained for large concentrations, see Fig. 5(d). Finally recent results on 3D aggregation lead to similar patterns as observed [23,24] with fractals, random dendrites, droplets, and gas.

ACKNOWLEDGMENT

The authors would like to thank Dr. Philippe Depondt from University Paris 6 for useful criticisms.

[1] C. Bréchignac, Ph. Cahuzac, F. Carlier, J. Leroux, A. Masson, B. Yoon, and U. Landman, Eur. Phys. J. D **16**, 265 (2001).
[2] S. H. Cohen and M. L. Lightbody, *Atomic Force Microscopy/ Scanning Tunneling Microscopy* (Kluwer, Amsterdam, 2002), Vol. 3.
[3] H. Brune, Surf. Sci. Rep. **31**, 121 (1998).
[4] H. Brune, H. Röder, C. Boragno, and K. Kern, Phys. Rev. Lett. **73**, 1955 (1994).
[5] A. Zangwill, *Physics at Surfaces* (Cambridge University Press, Cambridge, 1988).
[6] T. A. Witten and L. M. Sander, Phys. Rev. Lett. **47**, 1400 (1981).
[7] P. Meakin, Phys. Scr. **46**, 295 (1992).
[8] M. Filoche and B. Sapoval, Phys. Rev. Lett. **85**, 5118 (2000).
[9] M. E. J. Newman and G. T. Barkema, *Monte Carlo Methods in Statistical Physics* (Oxford University Press, Oxford, 1999).
[10] *Pulsed Laser Deposition of Thin Films*, edited by D. B. Chrisey and G. K. Hubler (Wiley, New York, 1994).
[11] S. W. Koch, R. C. Desai, and F. F. Abraham, Phys. Rev. A **27**, 2152 (1983).
[12] B. A. Korgel and D. Fitzmaurice, Phys. Rev. Lett. **80**, 3531 (1998).
[13] Ph. Depondt, A. Ghazali, and J.-C. S. Lévy, Surf. Sci. **419**, 29 (1998).
[14] V. A. Shchukin and D. Bimberg, Rev. Mod. Phys. **71**, 1125 (1999).
[15] W. Lu and Z. Suo, Phys. Rev. B **65**, 085401 (2002).
[16] C. J. Smitthells, *Metals Reference Book* (London Butterworths, London, 1967), Vol. 3.
[17] S. Tan, A. Ghazali, and J.-C. S. Lévy, Surf. Sci. **392**, 163 (1997).
[18] E. H. A de Hoog, W. K. Kegel, A. van Blaaderen, and H. N. W. Lekkerkerker, Phys. Rev. E **64**, 021407 (2001).
[19] W. Ostwald, Z. Phys. Chem., Stoechiom. Verwandtschaftsl. **22**, 289 (1897).
[20] J. Friedel, J. Phys. (Paris) **35**, L59 (1974); S. Alexander and J. McTague, Phys. Rev. Lett. **41**, 702 (1978).
[21] H. A. Makse, J. S. de Andrade, M. Batty, S. Havlin, and H. E. Stanley, Phys. Rev. E **58**, 7054 (1998).
[22] M. A. Kessler and B. T. Werner, Science **299**, 380 (2003).
[23] A. Ghazali and J.-C. S. Lévy, Phys. Lett. A **228**, 291 (1997).
[24] P. Mitchell and M. Frenkach, Phys. Rev. E **67**, 061407 (2003).